Occlusion of Diblock Copolymer-Modified Gold Nanoparticles Generates Diabolo-Shaped Au@ZnO Nanocomposite Crystals with Enhanced Photocatalytic Properties

Yingxiang Dong, Ziqing Liu, Yin Ning, Steven P. Armes* and Dan Li*

Guangdong Provincial Key Laboratory of Functional Supramolecular Coordination Materials and Applications, Jinan University, Guangzhou 510632, People's Republic of China

College of Chemistry and Materials Science, Jinan University, Guangzhou 510632, People's Republic of China

Department of Chemistry, University of Sheffield, Brook Hill, Sheffield, South Yorkshire S3 7HF, UK

ABSTRACT. Double-hydrophilic diblock copolymers have been extensively used as additives to tune the growth of inorganic crystals in aqueous media. However, there have been no reports of how double-hydrophilic diblock copolymer-decorated nanoparticles influence the morphology, structure and properties of such crystals. Herein, a well-defined poly(ammonium 2-sulfatoethyl methacrylate)-poly(glycerol monomethacrylate) diblock copolymer is prepared by RAFT polymerization and then adsorbed onto the surface of gold nanoparticles via its dithiobenzoate end-group to form sterically-stabilized nanoparticles. The growth of ZnO crystals in the presence of such nanoparticles leads to their occlusion, producing Au@ZnO nanocomposite crystals with a remarkable diabolo morphology. Furthermore, such Au@ZnO crystals enable the rapid photocatalytic degradation of a model organic dye (rhodamine B) when subjected to visible light irradiation. This study opens up a new avenue for the design of diblock copolymer-stabilized nanoparticles to enable the construction of organic-inorganic nanocomposite crystals that exhibit emergent properties.

Introduction

Double-hydrophilic diblock copolymers are well-known to be effective crystal growth modifiers.[1-4] Typically, one of the two blocks interacts with the crystal phase while the other acts as a steric stabilizer.[5-8] Preferential adsorption of copolymer chains at a specific crystal facet leads to suppression of the corresponding directional growth, thus conferring control over both crystal dimensions and morphology.[9-10] In recent years, various amphiphilic diblock copolymer nanoparticles have been employed as crystal growth additives: this approach has produced a range of nanocomposite materials in which the guest organic nanoparticles are densely occluded within host inorganic crystals.[11-13] Similar results have been achieved using polymer-stabilized

inorganic nanoparticles and even copolymer-stabilized oil droplets.[14-18] It is remarkable that a wide range of hybrid materials can be designed using such a straightforward, efficient method.[19-22] Unlike diblock copolymer nanoparticles, double-hydrophilic diblock copolymers are molecularly dissolved in aqueous solution. This is an important distinction, because the latter species can diffuse faster to the growing crystal surface.[23-24] Hence double-hydrophilic diblock copolymers often exhibit a more profound effect on the crystal size and morphology. However, incorporation of *functional* nanoparticles is more likely to lead to the resulting nanocomposite crystals possessing emergent properties.[25-29]

In the present study, we sought to combine the advantages of double-hydrophilic diblock copolymers and nanoparticles for the rational design of new nanocomposite crystals with controllable size, morphology, chemical composition and properties. More specifically, we employed reversible addition-fragmentation chain transfer (RAFT) polymerization to prepare a new double-hydrophilic diblock copolymer: poly(ammonium 2-sulfatoethyl methacrylate)$_{50}$-poly(glycerol monomethacrylate)$_{49}$ (denoted as S_{50}-G_{49} for brevity, where the subscripts refer to the mean degrees of polymerization of each block).[30-31] The dithiobenzoate group located at the end of the G_{49} block promotes the adsorption of such anionic-neutral copolymers onto gold nanoparticles, resulting in the formation of sterically-stabilized gold nanoparticles (see **Figure 1**). Subsequently, crystallization of zinc oxide (ZnO) in the presence of such S_{50}-G_{49}-Au nanoparticles results in the formation of a remarkable diabolo morphology in which S_{50}-G_{49}-Au nanoparticles are occluded within the inorganic crystalline matrix. Finally, the photocatalytic properties of such S_{50}-G_{49}-Au@ZnO diabolo crystals are briefly explored in the context of the visible light-induced degradation of a model organic dye (rhodamine B, or RhB). This study highlights a new synthetic approach to functional nanocomposite crystals.

Results and Discussion

Synthesis and Characterization of S_{50}-G_{49}-Au Nanoparticles

First, poly(ammonium 2-sulfatoethyl methacrylate)$_{50}$ (denoted as S_{50}) was prepared by RAFT polymerization. This anionic precursor was subsequently chain-extended using glycerol monomethacrylate to produce a poly(ammonium 2-sulfatoethyl methacrylate)$_{50}$-poly(glycerol monomethacrylate)$_{49}$ diblock copolymer in aqueous media (see **Figure 1** and **Figure S1**, detailed synthesis protocols are provided in the Supporting Information). Aqueous gel permeation chromatography (GPC) analysis indicated that both S_{50} and S_{50}-G_{49} had relatively narrow molecular weight distributions ($M_w/M_n < 1.25$, see **Figure S2**). This S_{50}-G_{49} copolymer was then used to modify gold nanoparticles to produce S_{50}-G_{49}-Au nanoparticles (see **Figure 2a**). Here the anionic S_{50} block is located within the outer coronal layer while the G_{49} block lies close to the gold cores: this is because the latter block bears the dithiobenzoate end-group that adsorbs onto the gold surface (see cartoon in **Figure 1**).[32] Thermogravimetric analysis (TGA) indicated an S_{50}-G_{49} copolymer content of ~ 64 wt.% (**Figure S3**). Given that transmission electron microscopy (TEM) studies indicate a mean core diameter of 4.4 ± 1.0 nm for the gold nanoparticles (**Figure 2a**), this corresponds to an adsorbed amount of ~25 mg m^{-2}. As expected, surface modification of the gold nanoparticles with this S_{50}-G_{49} diblock copolymer leads to an increase in the mean hydrodynamic diameter, as determined by dynamic light scattering (DLS, see **Figure S4a**). Aqueous electrophoresis studies indicated a less negative zeta potential for S_{50}-G_{49}-Au nanoparticles in the presence of zinc ions, which suggests that Zn^{2+} ions bind to the anionic S_{50} block (see **Figure S4b**).

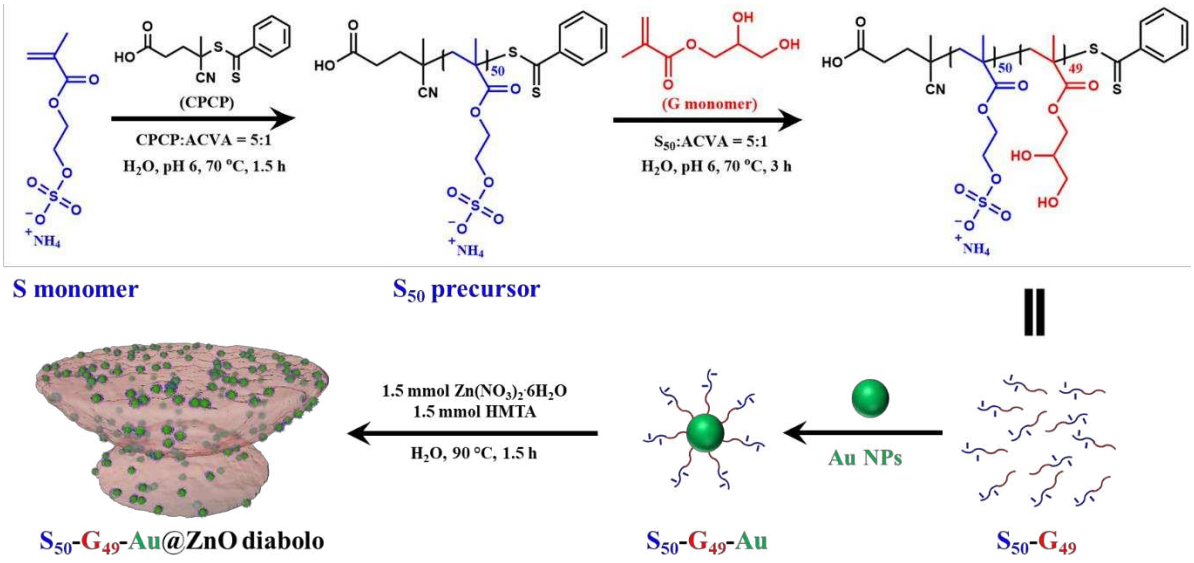

Figure 1. Synthesis of the poly(ammonium 2-sulfatoethyl methacrylate)$_{50}$-poly(glycerol monomethacrylate)$_{49}$ (S_{50}-G_{49}) double-hydrophilic diblock copolymer via RAFT aqueous solution polymerization and schematic representation of the formation of S_{50}-G_{49}-Au@ZnO diabolo nanocomposite crystals via *in situ* occlusion of S_{50}-G_{49}-Au nanoparticles.

Occlusion of S_{50}-G_{49}-Au Nanoparticles into ZnO Crystals

The surface plasmon band for S_{50}-G_{49}-Au nanoparticles was red-shifted by 7 nm compared to that observed for the original citrate-stabilized Au nanoparticles (see **Figure 2b**). This is attributed to adsorption of the S_{50}-G_{49} copolymer chains.[32] Importantly, no additional red shift is observed in the presence of 15 mM $Zn(NO_3)_2$, which indicates good colloidal stability for the S_{50}-G_{49}-Au nanoparticles under such conditions.[19] This is important because colloidally unstable nanoparticles cannot be efficiently occluded within growing crystals.[16, 19] Moreover, control experiments confirmed that using dithiobenzoate-capped S_{50} homopolymer instead of the S_{50}-G_{49} diblock copolymer led to gold nanoparticle aggregation in the presence of 15 mM $Zn(NO_3)_2$ (see **Figure S5**). The enhanced colloidal stability exhibited by the S_{50}-G_{49}-Au nanoparticles is

attributed to the non-ionic G_{49} block, which can tolerate the presence of Zn^{2+} while conferring steric stabilization.[19]

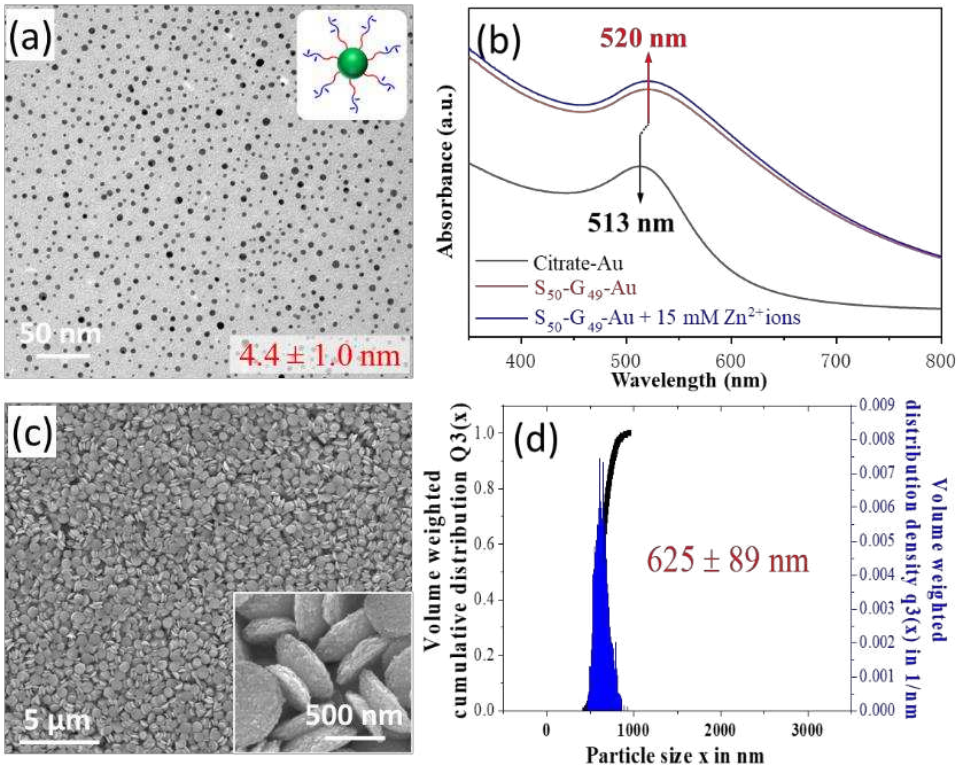

Figure 2. (a) TEM image recorded for S_{50}-G_{49}-Au nanoparticles with a number-average core diameter of 4.4 ± 1.0 nm, as determined by digital image analysis of 200 nanoparticles. The inset shows a schematic cartoon of a single S_{50}-G_{49}-Au nanoparticle; (b) Visible absorption spectra recorded for aqueous dispersions of citrate-Au, S_{50}-G_{49}-Au, and S_{50}-G_{49}-Au in the presence of 15 mM $Zn(NO_3)_2$. The surface plasmonic absorption band for S_{50}-G_{49}-Au is red-shifted compared to that for the original citrate-stabilized gold nanoparticles, confirming adsorption of the S_{50}-G_{49} copolymer. Furthermore, the visible absorption spectrum recorded for S_{50}-G_{49}-Au nanoparticles in the presence of Zn^{2+} ions is identical to that obtained for S_{50}-G_{49}-Au nanoparticles in deionized water, confirming good colloidal stability in the presence of Zn^{2+}; (c) SEM image recorded for S_{50}-G_{49}-Au@ZnO nanoparticles prepared in the presence of 0.15 g dm^{-3} S_{50}-G_{49}-Au nanoparticles (inset shows a magnified image depicting an unusual diabolo morphology); (d) volume-average particle size distribution recorded for S_{50}-G_{49}-Au@ZnO nanoparticles by analytical centrifugation (LUMiSizer instrument).

The S_{50}-G_{49}-Au nanoparticles (0.15 g dm^{-3}) were then used as additives for the precipitation of ZnO crystals in aqueous solution (see Supporting Information for further experimental details). Interestingly, scanning electron microscopy (SEM) studies indicated the formation of remarkably uniform ZnO particles with an unusual diabolo morphology (**Figure 2c**). Analytical centrifugation studies (LUMiSizer instrument) indicated a sphere-equivalent diameter of 625 ± 89 nm (**Figure 2d**), which is consistent with SEM observations. Subsequent studies confirmed that using higher S_{50}-G_{49}-Au nanoparticle concentrations led to narrower size distributions and superior colloidal stability for the S_{50}-G_{49}-Au@ZnO particles (see **Figures S6** and **S7**).

TEM studies confirmed such S_{50}-G_{49}-Au@ZnO particles have a concave, rough surface. Moreover, individual gold nanoparticles are clearly present at the surface of such S_{50}-G_{49}-Au@ZnO particles (see black dots in **Figure 3a**). Selected area electron diffraction (SAED) pattern indicated a wurtzite-type single ZnO crystal. The diffraction ring was assigned to Au(111), see **Figure 3b**. To confirm successful occlusion of the S_{50}-G_{49}-Au nanoparticles, S_{50}-G_{49}-Au@ZnO particles were embedded within a resin and then microtomed to produce thin sections. This enabled the internal structure of the S_{50}-G_{49}-Au@ZnO particles to be examined by TEM. **Figures 3c-3f** showed cross-sections prepared either perpendicular or parallel to the *c* axis of the S_{50}-G_{49}-Au@ZnO particles. Clearly, gold nanoparticles are distributed throughout the whole ZnO crystal. Moreover, lattice fringes were observed, which suggests that S_{50}-G_{49}-Au occlusion did not disturb the long-range order of the host crystal.[33] Powder X-ray diffraction studies indicated that S_{50}-G_{49}-Au@ZnO crystals formed in the presence of S_{50}-G_{49}-Au nanoparticles invariably exhibited a wurtzite structure and gold peaks could be detected at relatively high degrees of occlusion (see **Figure S8**). The extent of nanoparticle occlusion within S_{50}-G_{49}-Au@ZnO particles prepared in the presence of 0.15 g dm^{-3} S_{50}-G_{49}-Au nanoparticles was

determined to be 5.2% by mass, as judged by inductively-coupled plasma mass spectrometry (ICP-MS) studies.

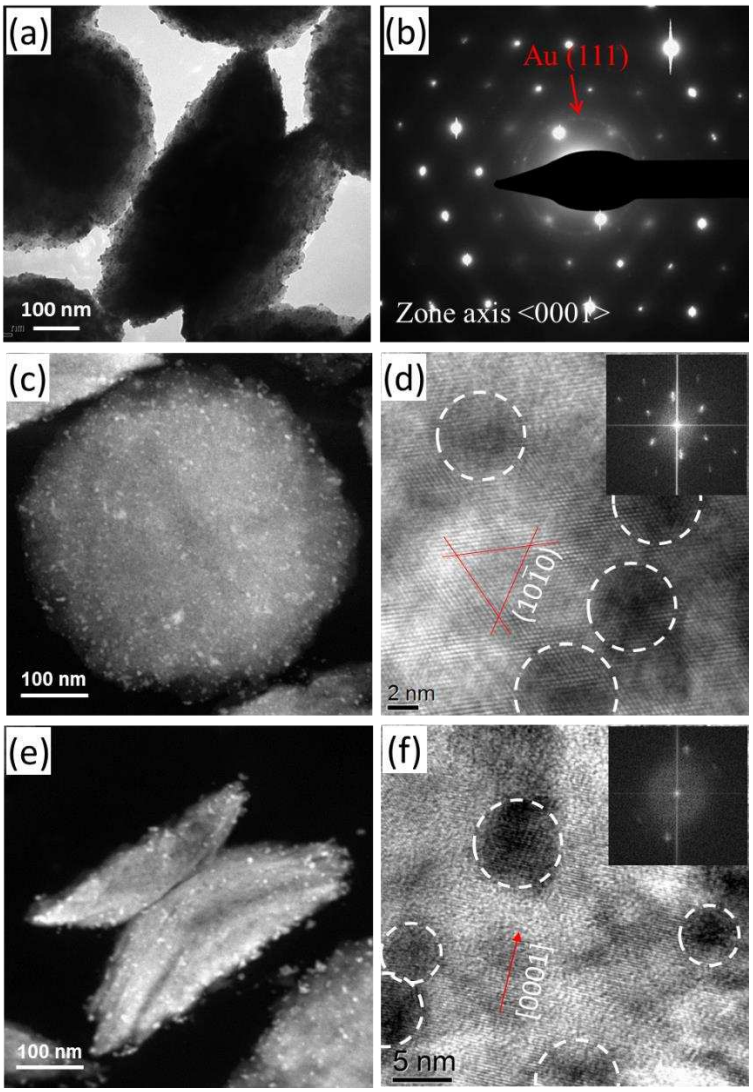

Figure 3. (a) TEM image of intact S_{50}-G_{49}-Au@ZnO particles precipitated in the presence of 0.15 g dm^{-3} S_{50}-G_{49}-Au nanoparticles; (b) selected area electron diffraction (SAED) pattern recorded for S_{50}-G_{49}-Au@ZnO particles; (c) HAADF-STEM images obtained perpendicular to the *c* axis for microtomed S_{50}-G_{49}-Au@ZnO particles; (d) TEM image recorded for the same sample examined in (c); (e) HAADF-STEM images obtained parallel to the *c* axis for microtomed S_{50}-G_{49}-Au@ZnO particles; (f) TEM images recorded for the same sample examined in (e). Insets in (d) and (f) show fast Fourier transform (FFT) patterns for the

corresponding images, indicating high crystallinity. Dashed white circles in (d) and (f) indicate occluded gold nanoparticles.

Mechanism for the Formation of S_{50}-G_{49}-Au@ZnO Nanoparticles with a Diabolo Morphology

A series of control experiments was conducted to examine the mechanism of formation for the diabolo-shaped S_{50}-G_{49}-Au@ZnO particles. In the absence of any additives, ZnO crystals exhibited a hexagonal prismatic rod morphology (see **Figure S9a**). In this case, twin rods grow outward from a central junction (**Figure S10**, further details are provided in the Supporting Information).[34] In addition, the Zn-rich cationic (0001) plane grows much faster than the six lateral non-polar $(10\bar{1}0)$ faces, which leads to a twinned rod structure.[35] The addition of S_{50} alone (denoted as S_{50}@ZnO) induced a significant change in the crystal morphology. Such S_{50}@ZnO crystals no longer possessed a rod-like structure but instead comprised an asymmetric twin structure (**Figure S9b**). This suggests that the anionic S_{50} chains strongly interact with the growing ZnO crystals (see **Figure S11** for the proposed mechanism). In contrast, ZnO crystals grown in the presence of poly(glycerol monomethacrylate) (G_{54}) alone retains its intrinsic rod-like morphology (**Figure S9c**), indicating that such non-ionic homopolymer chains do not affect the growth habit of ZnO (**Figure S12**). However, it is perhaps worth noting that the pendent *cis*-diol groups on poly(glycerol monomethacrylate) do chelate Zn^{2+} ions, which enables the efficient occlusion of G_{70}-Au nanoparticles within twinned rod-like ZnO crystals.[19] Interestingly, hexagonal ZnO plates were obtained in the presence of S_{50}-G_{49} alone. This is most likely because such diblock copolymer chains prevent the formation of twinned structure during the early stages of crystallization (see **Figure S13**, see detailed discussion in the Supporting Information). We

also attempted to incorporate S_{50}-Au nanoparticles into ZnO under the same conditions as those employed for the occlusion of S_{50}-G_{49}-Au nanoparticles. However, no occlusion could be achieved because the S_{50}-Au nanoparticles proved to be colloidally unstable in the presence of Zn^{2+}. Nevertheless, a dramatic change in the crystal morphology was observed (see **Figures S9e** and **S9f**).

Based on the above observations, the following mechanism was proposed for the formation of diabolo-shaped S_{50}-G_{49}-Au@ZnO crystals. Clearly, the S_{50} block directs the formation of diabolo morphology. Meanwhile, the non-ionic G_{49} block plays a key role in ensuring that the S_{50}-G_{49}-Au nanoparticles remain colloidally stable in the presence of Zn^{2+}, which is a prerequisite for their successful occlusion within ZnO crystals. During the formation of ZnO crystals, S_{50}-G_{49}-Au nanoparticles effectively adsorb onto the cationic (0001) plane and are gradually buried by growth of an ZnO overlayer. This is because the anionic S_{50} block ensures a strong electrostatic interaction between the nanoparticles and this crystal plane. As a result, the growth rate of the latter is significantly suppressed. This hypothesis is supported by the fact that the mean diabolo length for the S_{50}-G_{49}-Au@ZnO crystals is approximately 300 nm, which is much less than the ~2 μm dimensions of the ZnO control crystals (compare **Figure 2c** and **Figure S9a**). Meanwhile, the S_{50}-G_{49}-Au nanoparticles also prohibit the growth rate of $(10\bar{1}0)$ faces, particularly during the early stages of crystallization. However, this effect is gradually weakened as the ZnO crystals grow larger owing to the consumption of S_{50}-G_{49}-Au nanoparticles. This explains why the S_{50}-G_{49}-Au@ZnO particles eventually become concave in appearance.

Photocatalytic Degradation of a Model Organic Dye via Visible Light Irradiation

Close inspection of the TEM images shown in **Figure 3** suggests that there is no discernible S_{50}-G_{49} layer between the gold nanoparticles and the crystalline matrix. This is because the ZnO grows throughout the diblock copolymer stabilizer chains and hence comes into intimate intact with the gold nanoparticle cores. In principle, this should promote efficient charge transfer between these two components. Indeed, X-ray photoelectron spectroscopy (XPS) studies confirmed that two signals corresponding to Au 4f electronic states are shifted to lower binding energies for the S_{50}-G_{49}-Au@ZnO particles. Correspondingly, two Zn 2p signals are shifted to higher values (see **Figures 4a** and **4b**). Additionally, these Au 4f signals become more intense when using higher S_{50}-G_{49}-Au nanoparticle concentrations, indicating a higher degree of occlusion. This is consistent with IR spectroscopy studies, where the ester carbonyl band at 1723 cm^{-1} become gradually more intense for ZnO crystals prepared using higher concentrations of S_{50}-G_{49}-Au nanoparticles (**Figure 4c**).

UV-visible absorption spectra indicated that the maximum absorption band is red-shifted from the near-UV region (377 nm) into the visible region (440 nm). Moreover, this band gradually broadens for S_{50}-G_{49}-Au@ZnO particles prepared when using higher concentrations of S_{50}-G_{49}-Au nanoparticles (see **Figure 4d**). These features are most probably attributed to the morphological change induced by the incorporation of the S_{50}-G_{49}-Au nanoparticles.[36] The characteristic strong plasmonic absorption band for gold nanoparticles was not detected. Presumably, this is because surface plasmon resonance is significantly weakened as electronic charge is rapidly transferred to the ZnO matrix.[37-38]

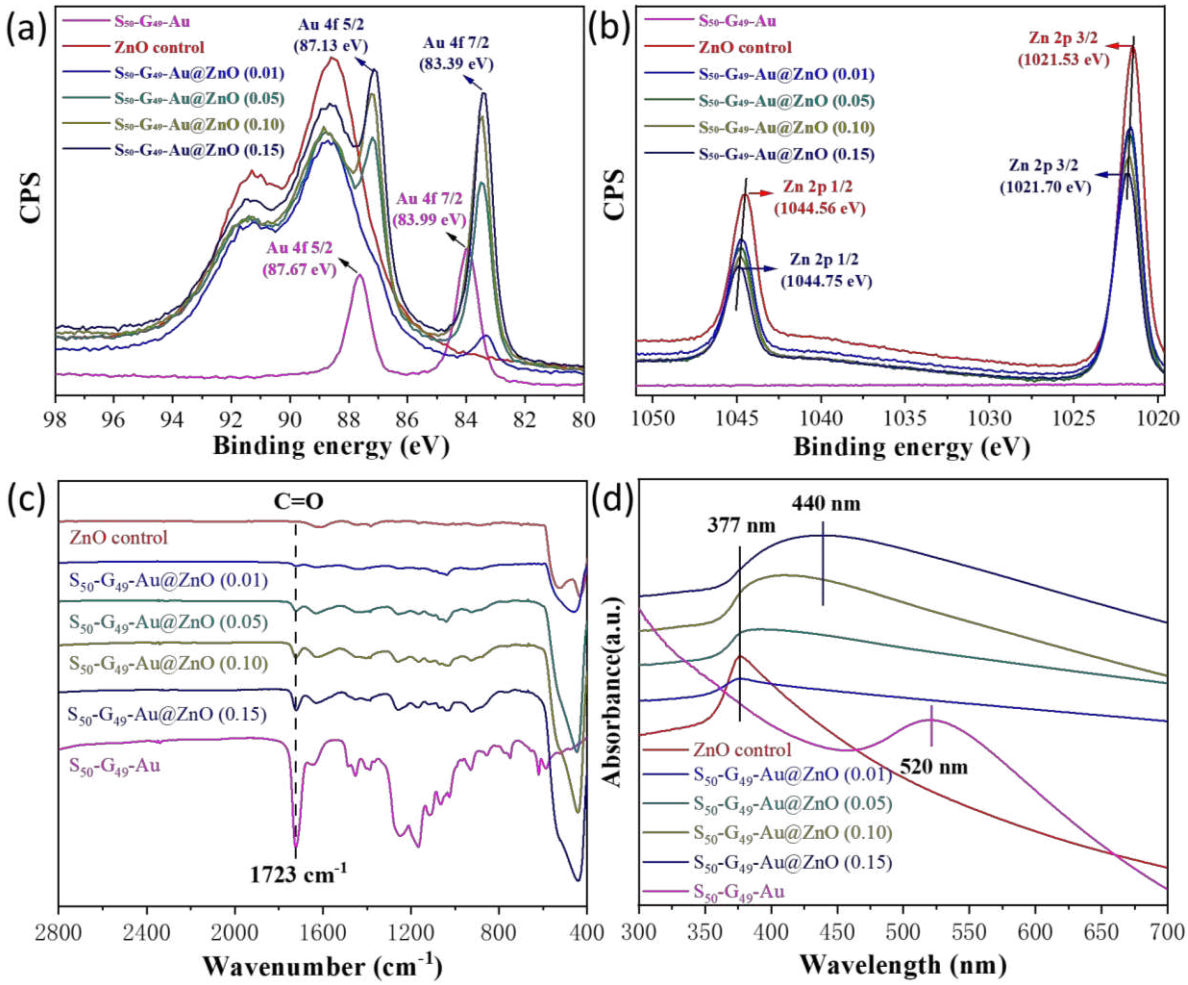

Figure 4. High-resolution X-ray photoelectron spectra recorded for various S_{50}-G_{49}-Au@ZnO crystals and various appropriate reference materials: (a) Au 4f; (b) Zn 2p. (c) FTIR spectra and (d) UV-visible absorption spectra recorded for a ZnO control, the S_{50}-G_{49}-Au nanoparticles alone and four example of S_{50}-G_{49}-Au@ZnO particles prepared using varying concentrations of S_{50}-G_{49}-Au nanoparticles (see individual labels for further details).

Inspired by the above observations, we then explored the photocatalytic property of these S_{50}-G_{49}-Au@ZnO particles for the decomposition of a model dye, rhodamine B, subjected to visible

light irradiation. **Figure 5a** indicates that only a minor fraction of RhB dye molecules (~10%) are decomposed during visible light irradiation for 3 h conducted either in the presence of S_{50}-G_{49}-Au nanoparticles or in the absence of any additives. These observations are consistent with the well-known self-degradation of this particular dye under visible light in aqueous media.[39] In another control experiment, a faster rate of dye degradation was observed in the presence of the rod-like ZnO particles. This is the result of RhB-induced sensitization of ZnO, as previous reported.[40] The mechanism is depicted in **Figure 5b** (see **Route 1**). First, RhB molecules are activated by visible light to generate excited electron and holes. These electrons are transferred to the ZnO conduction band and interact with oxygen to form radicals, leading to dye decomposition. Remarkably, more than 95 % RhB dye is decomposed by visible light irradiation for 3 h in the presence of S_{50}-G_{49}-Au@ZnO particles. This significant enhancement in photocatalytic efficiency cannot be solely attributed to dye-induced sensitization (**Route 1**). The incorporation of S_{50}-G_{49}-Au nanoparticles undoubtedly plays a vital role in achieving such a significant improvement. We propose the following additional mechanism (see **Route 2** in **Figure 5b**). First, visible light is absorbed by the S_{50}-G_{49}-Au@ZnO particles, which absorb visible light intensely in the 400~600 nm range (see **Figure 4d**) and electron-hole pairs are generated in the vicinity of the gold nanoparticles. The electrons are rapidly transferred into the ZnO conduction band, aided by the intimate contact between the guest gold nanoparticles and the host ZnO crystals. This spatial separation of charge minimizes recombination between electrons and holes, thus significantly promoting photocatalytic behavior. In addition, the change from a rod-like to a diabolo morphology exposes electronegative oxygen atoms at the concave surface of the S_{50}-G_{49}-Au@ZnO particles. This should facilitate the electrostatic adsorption of cationic

RhB molecules and also promote the transfer of excited electrons to ZnO (**Route 1**), thus enhancing the photocatalytic efficiency.

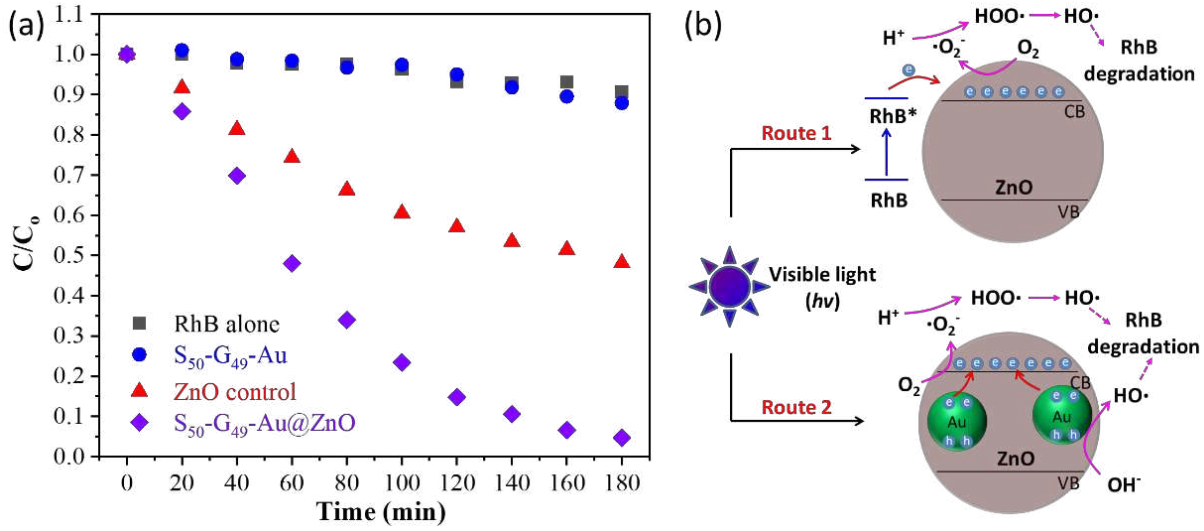

Figure 5. (a) Rate of photodegradation of a model organic dye (rhodamine B, or RhB) under visible light irradiation under the following conditions: dye alone (black data set), S_{50}-G_{49}-Au nanoparticles (blue data set), ZnO crystals alone (red data set), and S_{50}-G_{49}-Au@ZnO (purple data set). (b) Schematic representation of two proposed mechanisms for photodegradation of RhB under visible light. Route 1 refers to dye-induced sensitization whereby the excited electrons are generated from dye molecules subjected to visible light irradiation. In contrast, Route 2 involves the generation of electron-hole pairs at the Au nanoparticles and the electrons are immediately transferred into ZnO due to the intimate contact between the occluded gold nanoparticles and the ZnO host crystal. Hence, this rapid spatial separation of electrons and holes significantly promotes the photocatalytic property.

Conclusions

The design of bespoke nanoparticles for efficient occlusion within inorganic crystals has traditionally focused on optimizing the nanoparticle surface chemistry.[41-42] Typically, this

involves using a single homopolymer as a steric stabilizer.[36, 43-44] In the present study, a new anionic-neutral double hydrophilic diblock copolymer (S_{50}-G_{49}) has been prepared via RAFT polymerization. This copolymer was used to produce S_{50}-G_{49}-Au nanoparticles with a core-shell morphology. Subsequent incorporation of such model nanoparticles into ZnO led to the formation of S_{50}-G_{49}-Au@ZnO crystals with a remarkable 'diabolo' morphology. The anionic S_{50} block ensured a strong interaction between the nanoparticles and the host crystals while the non-ionic G_{49} block enhances colloidal stability and thus facilitates nanoparticle incorporation. Such occlusion dramatically changes the growth habit of ZnO crystals and also generated new nanocomposite crystals with enhanced photocatalytic properties, as evidenced by visible light photodegradation of a model dye (rhodamine B). In principle, this approach suggests a generic, efficient route for the preparation of a series of novel functional hybrid materials with controllable compositions, morphologies and physicochemical properties.

ASSOCIATED CONTENT

Supporting Information. Experimental details and characterization methods, additional Figures and mechanism discussion.

AUTHOR INFORMATION

Corresponding Author

Yin Ning--Guangdong Provincial Key Laboratory of Functional Supramolecular Coordination Materials and Applications, Jinan University, Guangzhou 510632, People's Republic of China; College of Chemistry and Materials Science, Jinan University, Guangzhou 510632, People's Republic of China. ORCID: 0000-0003-1808-3513; Email: yinning@jnu.edu.cn

Steven P. Armes--Department of Chemistry, University of Sheffield, Brook Hill, Sheffield, South Yorkshire S3 7HF, UK; ORCID: 0000-0002-8289-6351; Email: s.p.armes@sheffield.ac.uk

Authors

Yingxiang Dong--Guangdong Provincial Key Laboratory of Functional Supramolecular Coordination Materials and Applications, Jinan University, Guangzhou 510632, People's Republic of China; College of Chemistry and Materials Science, Jinan University, Guangzhou 510632, People's Republic of China.

Ziqing Liu--Guangdong Provincial Key Laboratory of Functional Supramolecular Coordination Materials and Applications, Jinan University, Guangzhou 510632, People's Republic of China; College of Chemistry and Materials Science, Jinan University, Guangzhou 510632, People's Republic of China.

Dan Li--Guangdong Provincial Key Laboratory of Functional Supramolecular Coordination Materials and Applications, Jinan University, Guangzhou 510632, People's Republic of China; College of Chemistry and Materials Science, Jinan University, Guangzhou 510632, People's Republic of China.

Notes

The authors declare no competing financial interest.

ACKNOWLEDGMENT

Y.N gratefully thanks the financial supports from the National Natural Science Foundation of China (22101100) and the Fundamental Research Funds for the Central Universities (21621032).

S.P.A acknowledges an EPSRC Established Career Particle Technology Fellowship (EP/R003009).

REFERENCES

1. Cölfen, H., Double‐hydrophilic block copolymers: synthesis and application as novel surfactants and crystal growth modifiers. *Macromol. Rapid Commun.* **2001,** *22* (4), 219-252.
2. Zhang, D.; Qi, L.; Ma, J.; Cheng, H., Formation of silver nanowires in aqueous solutions of a double-hydrophilic block copolymer. *Chem. Mater.* **2001,** *13* (9), 2753-2755.
3. Yu, S.-H.; Cölfen, H., Bio-inspired crystal morphogenesis by hydrophilic polymers. *J. Mater. Chem.* **2004,** *14* (14), 2124-2147.
4. Kulak, A. N.; Iddon, P.; Li, Y.; Armes, S. P.; Cölfen, H.; Paris, O.; Wilson, R. M.; Meldrum, F. C., Continuous structural evolution of calcium carbonate particles: a unifying model of copolymer-mediated crystallization. *J. Am. Chem. Soc.* **2007,** *129* (12), 3729-3736.
5. Qi, L.; Cölfen, H.; Antonietti, M., Crystal design of barium sulfate using double‐hydrophilic block copolymers. *Angew. Chem. Int. Ed.* **2000,** *39* (3), 604-607.
6. Qi, L.; Cölfen, H.; Antonietti, M., Control of Barite Morphology by Double-Hydrophilic Block Copolymers. *Chem. Mater.* **2000,** *12* (8), 2392-2403.
7. Cölfen, H.; Antonietti, M., Crystal Design of Calcium Carbonate Microparticles Using Double-Hydrophilic Block Copolymers. *Langmuir* **1998,** *14* (3), 582-589.
8. Zhang, D.; Qi, L.; Ma, J.; Cheng, H., Morphological Control of Calcium Oxalate Dihydrate by a Double-Hydrophilic Block Copolymer. *Chem. Mater.* **2002,** *14* (6), 2450-2457.
9. Yu, S. H.; Cölfen, H.; Hartmann, J.; Antonietti, M., Biomimetic crystallization of calcium carbonate spherules with controlled surface structures and sizes by double‐hydrophilic block copolymers. *Adv. Funct. Mater.* **2002,** *12* (8), 541-545.
10. Hwang, J.; Heil, T.; Antonietti, M.; Schmidt, B. V., Morphogenesis of metal–organic mesocrystals mediated by double hydrophilic block copolymers. *J. Am. Chem. Soc.* **2018,** *140* (8), 2947-2956.
11. Ning, Y.; Armes, S. P., Efficient Occlusion of Nanoparticles within Inorganic Single Crystals. *Acc. Chem. Res.* **2020,** *53*, 1176–1186.
12. Ren, J.; Liu, Y.; Li, H., Incorporating polymers within a single‐crystal: From heterogeneous structure to multiple functions. *J. Polym. Sci.* **2021,** *doi.org/10.1002/pol.20210408*.
13. Kim, Y.-Y.; Ganesan, K.; Yang, P.; Kulak, A. N.; Borukhin, S.; Pechook, S.; Ribeiro, L.; Kröger, R.; Eichhorn, S. J.; Armes, S. P., An artificial biomineral formed by incorporation of copolymer micelles in calcite crystals. *Nat. Mater.* **2011,** *10* (11), 890-896.
14. Kulak, A. N.; Semsarilar, M.; Kim, Y.-Y.; Ihli, J.; Fielding, L. A.; Cespedes, O.; Armes, S. P.; Meldrum, F. C., One-pot synthesis of an inorganic heterostructure: uniform occlusion of magnetite nanoparticles within calcite single crystals. *Chem. Sci.* **2014,** *5* (2), 738-743.
15. Ning, Y.; Meldrum, F. C.; Armes, S. P., Efficient occlusion of oil droplets within calcite crystals. *Chem. Sci.* **2019,** *10* (39), 8964-8972.
16. Kim, Y.-Y.; Darkins, R.; Broad, A.; Kulak, A. N.; Holden, M. A.; Nahi, O.; Armes, S. P.; Tang, C. C.; Thompson, R. F.; Marin, F., Hydroxyl-rich macromolecules enable the bio-inspired synthesis of single crystal nanocomposites. *Nat. Commun.* **2019,** *10* (1), 5682.

17. Sun, K.; Liu, M.; Pei, J.; Li, D.; Ding, C.; Wu, K.; Jiang, H.-L., Incorporating Transition-Metal Phosphides Into Metal-Organic Frameworks for Enhanced Photocatalysis. *Angew. Chem. Int. Ed.* **2020,** *59* (50), 22749-22755.
18. Xiao, J. D.; Shang, Q.; Xiong, Y.; Zhang, Q.; Luo, Y.; Yu, S. H.; Jiang, H. L., Boosting photocatalytic hydrogen production of a metal–organic framework decorated with platinum nanoparticles: The platinum location matters. *Angew. Chem. Int. Ed.* **2016,** *55* (32), 9389-9393.
19. Ning, Y.; Fielding, L. A.; Nutter, J.; Kulak, A. N.; Meldrum, F. C.; Armes, S. P., Spatially controlled occlusion of polymer‐stabilized gold nanoparticles within ZnO. *Angew. Chem. Int. Ed.* **2019,** *58* (13), 4302-4307.
20. Yang, Q.; Xu, Q.; Jiang, H.-L., Metal–organic frameworks meet metal nanoparticles: synergistic effect for enhanced catalysis. *Chem. Soc. Rev.* **2017,** *46* (15), 4774-4808.
21. Liu, Y.; Zang, H.; Wang, L.; Fu, W.; Yuan, W.; Wu, J.; Jin, X.; Han, J.; Wu, C.; Wang, Y., Nanoparticles incorporated inside single-crystals: enhanced fluorescent properties. *Chem. Mater.* **2016,** *28* (20), 7537-7543.
22. Ning, Y.; Han, Y.; Han, L.; Derry, M. J.; Armes, S. P., Exerting Spatial Control During Nanoparticle Occlusion within Calcite Crystals. *Angew. Chem. Int. Ed.* **2020,** *59*, 17966-17973.
23. Hendley IV, C. T.; Fielding, L. A.; Jones, E. R.; Ryan, A. J.; Armes, S. P.; Estroff, L. A., Mechanistic insights into diblock copolymer nanoparticle–crystal interactions revealed via in situ atomic force microscopy. *J. Am. Chem. Soc.* **2018,** *140* (25), 7936-7945.
24. Cho, K. R.; Kim, Y.-Y.; Yang, P.; Cai, W.; Pan, H.; Kulak, A. N.; Lau, J. L.; Kulshreshtha, P.; Armes, S. P.; Meldrum, F. C., Direct observation of mineral–organic composite formation reveals occlusion mechanism. *Nat. Commun.* **2016,** *7* (1), 10187.
25. Ning, Y.; Han, L.; Derry, M. J.; Meldrum, F. C.; Armes, S. P., Model anionic block copolymer vesicles provide important design rules for efficient nanoparticle occlusion within calcite. *J. Am. Chem. Soc.* **2019,** *141* (6), 2557-2567.
26. Douverne, M.; Ning, Y.; Tatani, A.; Meldrum, F. C.; Armes, S. P., How Many Phosphoric Acid Units Are Required to Ensure Uniform Occlusion of Sterically Stabilized Nanoparticles within Calcite? *Angew. Chem. Int. Ed.* **2019,** *58* (26), 8692-8697.
27. Ning, Y.; Whitaker, D. J.; Mable, C. J.; Derry, M. J.; Penfold, N. J.; Kulak, A. N.; Green, D. C.; Meldrum, F. C.; Armes, S. P., Anionic block copolymer vesicles act as Trojan horses to enable efficient occlusion of guest species into host calcite crystals. *Chem. Sci.* **2018,** *9* (44), 8396-8401.
28. Liu, Y.; Yuan, W.; Shi, Y.; Chen, X.; Wang, Y.; Chen, H.; Li, H., Functionalizing Single Crystals: Incorporation of Nanoparticles Inside Gel‐Grown Calcite Crystals. *Angew. Chem. Int. Ed.* **2014,** *53*, 4127-4131.
29. Lu, G.; Li, S.; Guo, Z.; Farha, O. K.; Hauser, B. G.; Qi, X.; Wang, Y.; Wang, X.; Han, S.; Liu, X., Imparting functionality to a metal–organic framework material by controlled nanoparticle encapsulation. *Nat. Chem.* **2012,** *4* (4), 310-316.
30. Chiefari, J.; Chong, Y. K.; Ercole, F.; Krstina, J.; Jeffery, J.; Le, T. P. T.; Mayadunne, R. T. A.; Meijs, G. F.; Moad, C. L.; Moad, G.; Rizzardo, E.; Thang, S. H., Living Free-Radical Polymerization by Reversible Addition−Fragmentation Chain Transfer: The RAFT Process. *Macromolecules* **1998,** *31* (16), 5559-5562.
31. Semsarilar, M.; Perrier, S., 'Green'reversible addition-fragmentation chain-transfer (RAFT) polymerization. *Nat. Chem.* **2010,** *2* (10), 811-820.

32. Liang, M.; Lin, I.-C.; Whittaker, M. R.; Minchin, R. F.; Monteiro, M. J.; Toth, I., Cellular uptake of densely packed polymer coatings on gold nanoparticles. *ACS Nano* **2010,** *4* (1), 403-413.
33. Li, H.; Xin, H. L.; Muller, D. A.; Estroff, L. A., Visualizing the 3D internal structure of calcite single crystals grown in agarose hydrogels. *Science* **2009,** *326* (5957), 1244-1247.
34. Yu, Q.; Yu, C.; Yang, H.; Fu, W.; Chang, L.; Xu, J.; Wei, R.; Li, H.; Zhu, H.; Li, M., Growth of dumbbell-like ZnO microcrystals under mild conditions and their photoluminescence properties. *Inorg. Chem.* **2007,** *46* (15), 6204-6210.
35. Wang, Z. L., Zinc oxide nanostructures: growth, properties and applications. *J. Condens. Matter Phys.* **2004,** *16* (25), R829.
36. Ning, Y.; Fielding, L.; Andrews, T.; Growney, D.; Armes, S., Sulfate-based anionic diblock copolymer nanoparticles for efficient occlusion within zinc oxide. *Nanoscale* **2015,** *7* (15), 6691-6702.
37. Yi, Z.; Chen, J.; Luo, J.; Yi, Y.; Kang, X.; Ye, X.; Bi, P.; Gao, X.; Yi, Y.; Tang, Y., Surface-plasmon-enhanced band emission and enhanced photocatalytic activity of Au nanoparticles-decorated ZnO nanorods. *Plasmonics* **2015,** *10* (6), 1373-1380.
38. Yin, J.; Yue, C.; Zang, Y.; Chiu, C.-H.; Li, J.; Kuo, H.-C.; Wu, Z.; Li, J.; Fang, Y.; Chen, C., Effect of the surface-plasmon–exciton coupling and charge transfer process on the photoluminescence of metal–semiconductor nanostructures. *Nanoscale* **2013,** *5* (10), 4436-4442.
39. She, P.; Xu, K.; He, Q.; Zeng, S.; Sun, H.; Liu, Z., Controlled preparation and visible light photocatalytic activities of corn cob-like Au–ZnO nanorods. *J. Mater. Sci.* **2017,** *52* (6), 3478-3489.
40. Xiang, Q.; Yu, J.; Cheng, B.; Ong, H., Microwave‐hydrothermal preparation and visible‐light photoactivity of plasmonic photocatalyst Ag‐TiO2 nanocomposite hollow spheres. *Chem. Asian J.* **2010,** *5* (6), 1466-1474.
41. Ning, Y.; Fielding, L. A.; Ratcliffe, L. P.; Wang, Y.-W.; Meldrum, F. C.; Armes, S. P., Occlusion of sulfate-based diblock copolymer nanoparticles within calcite: effect of varying the surface density of anionic stabilizer chains. *J. Am. Chem. Soc.* **2016,** *138* (36), 11734-11742.
42. Ning, Y.; Fielding, L. A.; Doncom, K. E.; Penfold, N. J.; Kulak, A. N.; Matsuoka, H.; Armes, S. P., Incorporating Diblock Copolymer Nanoparticles into Calcite Crystals: Do Anionic Carboxylate Groups Alone Ensure Efficient Occlusion? *ACS Macro Lett.* **2016,** *5* (3), 311-315.
43. Ihli, J.; Levenstein, M. A.; Kim, Y.-Y.; Wakonig, K.; Ning, Y.; Tatani, A.; Kulak, A. N.; Green, D. C.; Holler, M.; Armes, S. P., Ptychographic X-ray tomography reveals additive zoning in nanocomposite single crystals. *Chem. Sci.* **2020,** *11* (2), 355-363.
44. Ning, Y.; Han, L.; Douverne, M.; Penfold, N. J.; Derry, M. J.; Meldrum, F. C.; Armes, S. P., What Dictates the Spatial Distribution of Nanoparticles within Calcite? *J. Am. Chem. Soc.* **2019,** *141* (6), 2481-2489.